

**Cell Reports, Volume 43**

**Supplemental information**

**Oligodendrocyte-derived LGI3 and its receptor**

**ADAM23 organize juxtaparanodal Kv1 channel**

**clustering for short-term synaptic plasticity**

**Yuri Miyazaki, Takeshi Otsuka, Yoko Yamagata, Toshihiro Endo, Makoto Sanbo, Hiromi Sano, Kenta Kobayashi, Hiroki Inahashi, Hans-Christian Kornau, Dietmar Schmitz, Harald Prüss, Dies Meijer, Masumi Hirabayashi, Yuko Fukata, and Masaki Fukata**

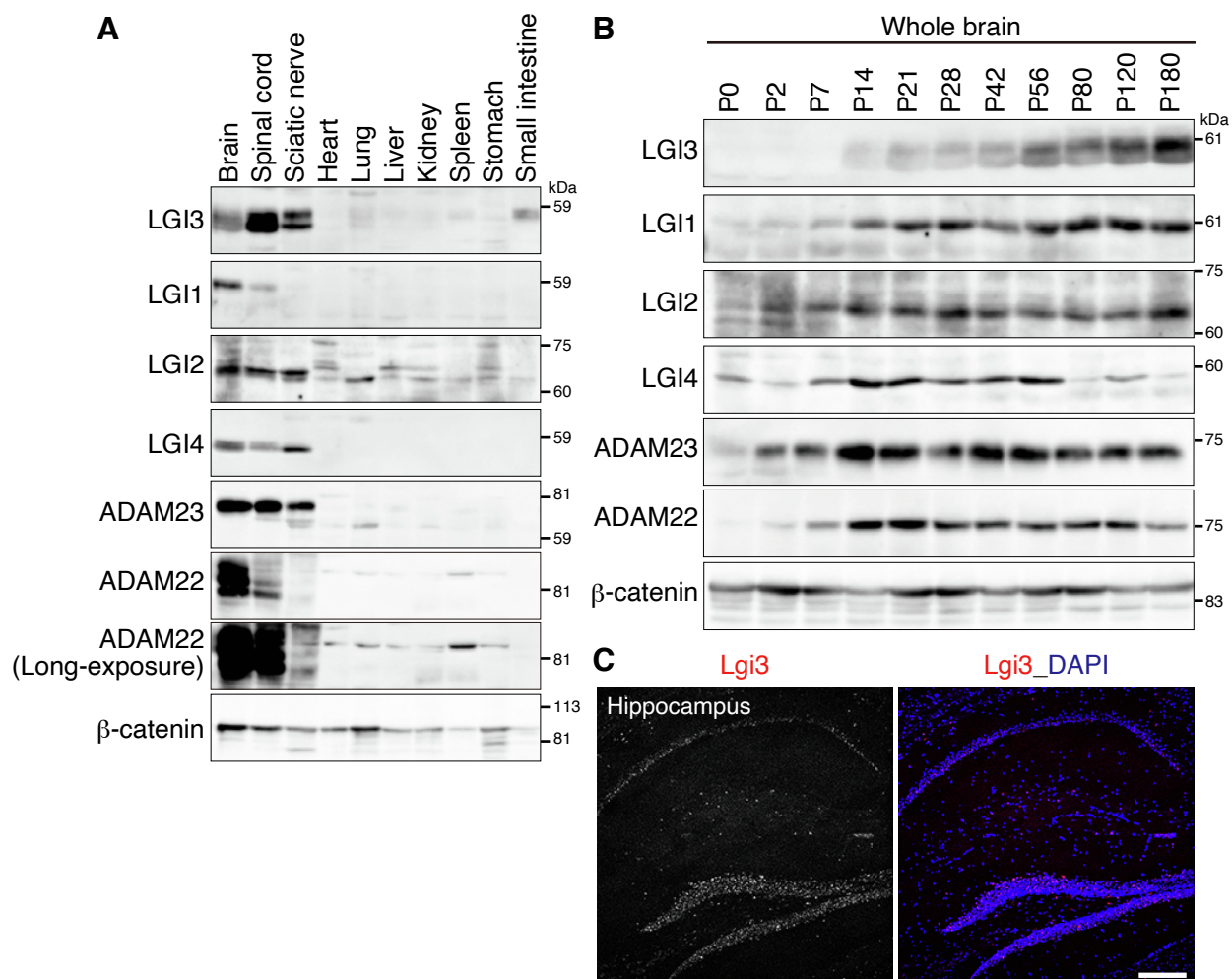


**Figure S1. Tissue and developmental expression profiles of LGI family members in mice, Related to Figure 1**

(A) Western blotting of various mouse tissue extracts (20 µg total protein each, P90 mouse) for LGI family and ADAM23 family proteins.

(B) Western blotting of mouse brain extracts from different postnatal ages (40 µg total protein each) for LGI family and ADAM23 family proteins.

(C) *Lgi3* mRNA is detected in neuronal cells of the mouse hippocampus (dentate granule cells and CA1 pyramidal neurons) by FISH analysis. Nuclear DNA was stained by DAPI. P125 mouse brain slice was used. Scale bar, 200 µm.

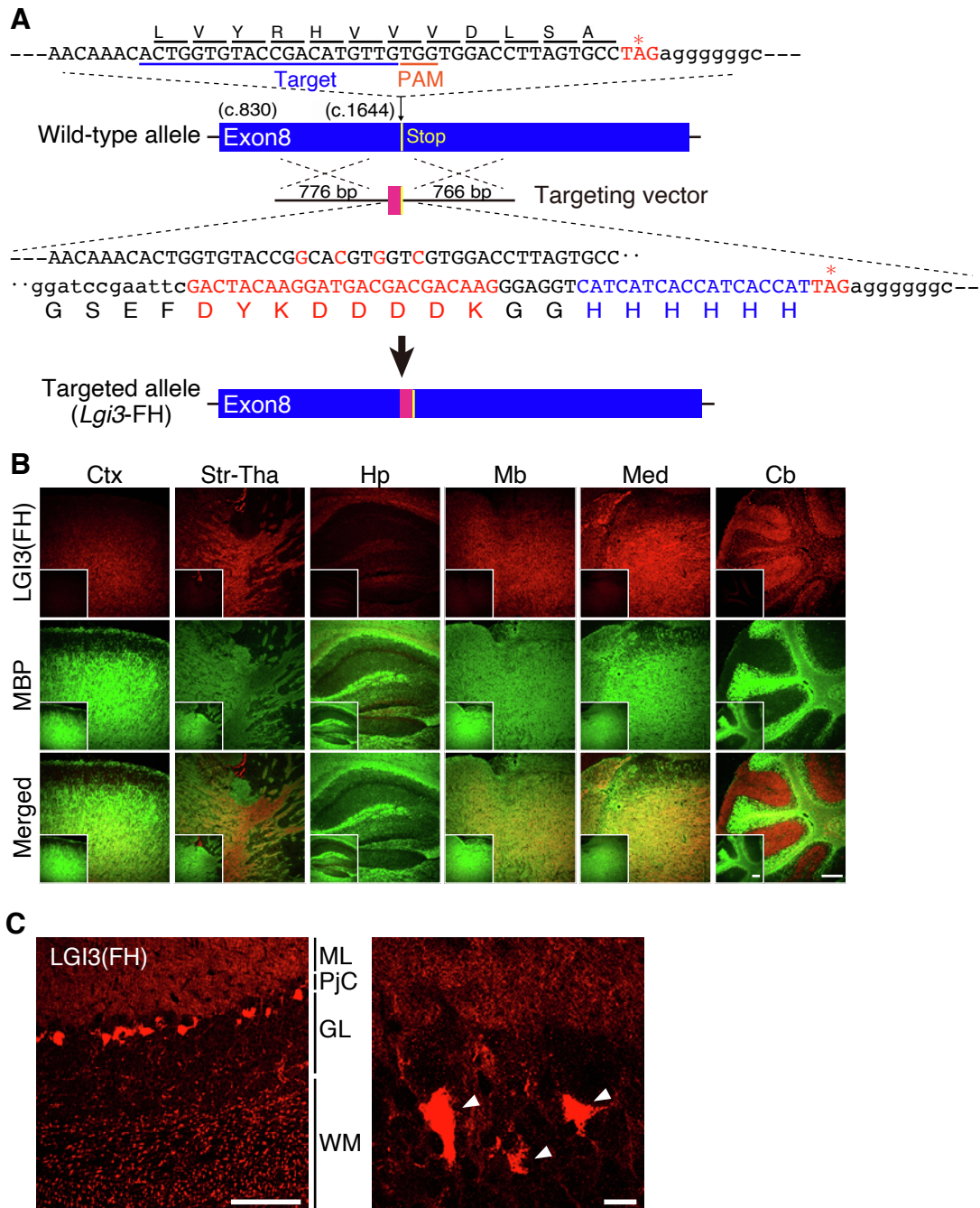


**Figure S2. LGI3 is localized in myelin-rich brain regions, cerebellar molecular layers, and basket cell terminals, Related to Figure 2**

(A) Targeting strategy for the *Lgi3*<sup>FH/FH</sup> knock-in allele by the CRISPR-Cas9 system. The targeting vector for the homology-directed repair has a FLAG-Hisx6 (FH) tag sequence (GSEFDYKDDDDDKGGHHHHHH) flanked by ~1.5 kb homology arms.

(B) LGI3-FH is largely colocalized with MBP in the various mouse brain regions. Fluorescence signals of FH antibody in *Lgi3*<sup>FH/FH</sup> mice are specific, as no signals are observed in wild-type mice (insets). Ctx cortex; Str, striatum; Tha, thalamus; Hp, hippocampus; Mb, midbrain; Med, medulla; Cb, cerebellum. Scale bar, 250  $\mu$ m.

(C) LGI3-FH is localized at the molecular layer (ML) and basket cell terminals (pinneau) in the mouse cerebellum. Note that paintbrush-like clusters of LGI3-FH are observed in the cerebellar white matter (WM) but not in the molecular layer (left). Magnified image shows the localization of LGI3-FH at pinneau (right, arrowheads). PjC, Purkinje cell layer; GL, granule cell layer. Scale bars, 100  $\mu$ m (left) and 10  $\mu$ m (magnified, right).

P166 (B) and P100 (C) mouse brain slices were used.

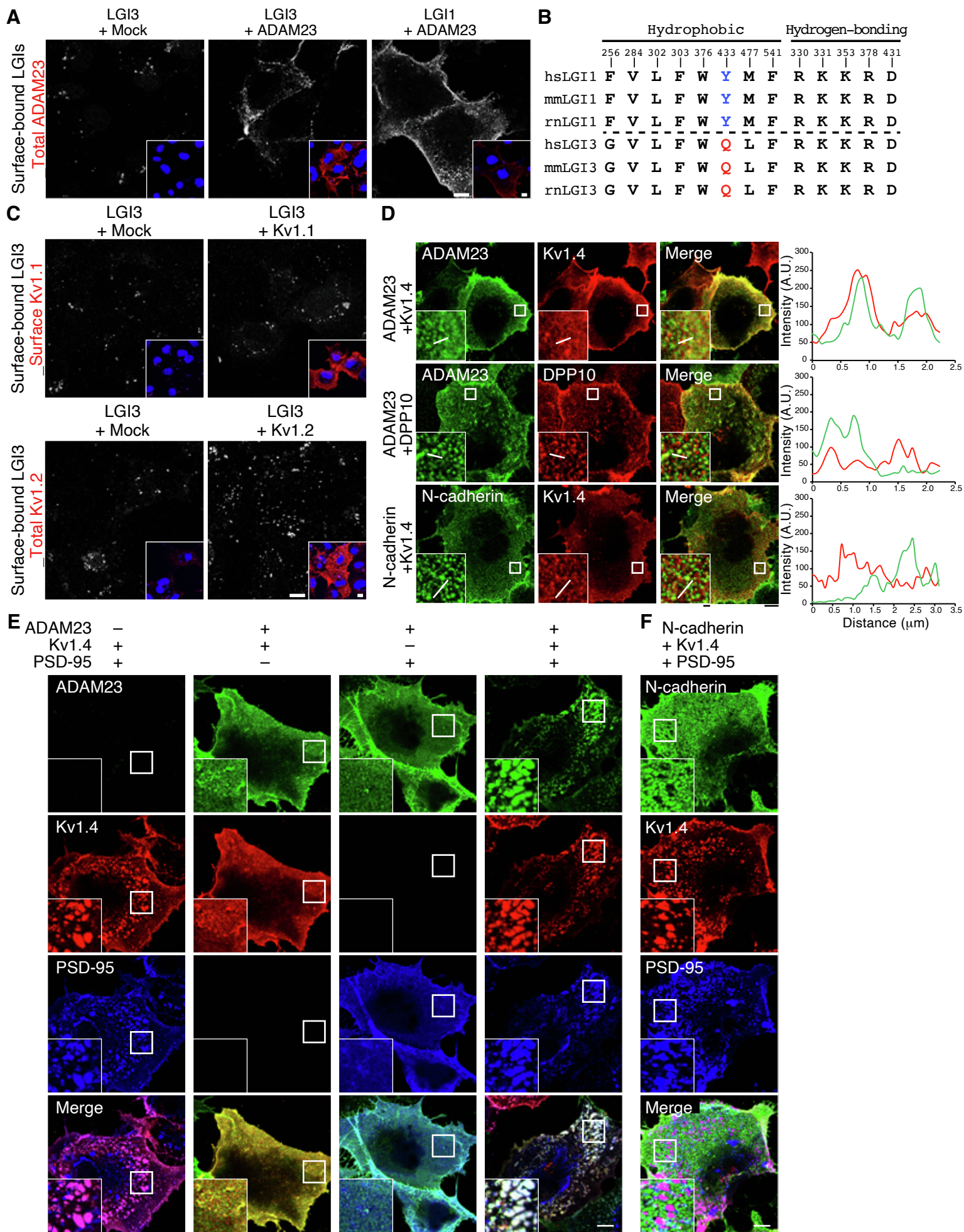


Figure S3 (related to Fig.3)

**Figure S3. LGI3 directly interacts with ADAM23 but not with Kv1 channels in vitro, Related to Figure 3**

**(A)** Cell-surface binding assay between LGI3 and ADAM23. COS7 cells were cotransfected with V5-tagged LGI3 or LGI1 (LGIs) and ADAM23 constructs. Surface-bound LGIs were live-stained with anti-V5 antibodies (grayscale). The total ADAM23 was stained after permeabilization (red, inset). The mock-cotransfected cells were used as a negative control for the surface binding of LGI3. Nuclear DNA was stained by Hoechst 33342 (blue). Scale bars, 10  $\mu\text{m}$ .

**(B)** Amino-acid residues of LGI1 responsible for the hydrophobic and hydrogen-bonding interactions with ADAM22 or ADAM23 are conserved in those of LGI3. Blue and red letters represent amino acid residues with distinct properties at the binding interface of LGI1 and LGI3, respectively. hs, Homo sapiens; mm, Mus musculus; rn, Rattus norvegicus.

**(C)** Cell-surface binding assay between LGI3 and Kv1 channels. COS7 cells were cotransfected with HA-tagged LGI3 and Kv1.1 (upper), or V5-tagged LGI3 and Kv1.2 (lower) constructs. Surface LGI3 (grayscale) and Kv1.1 were live-stained (red, inset) and total Kv1.2 was stained after permeabilization (red, inset). Nuclear DNA was stained by Hoechst 33342 (blue). Scale bars, 10  $\mu\text{m}$ .

**(D)** Cell surface co-localization analysis indicates the specific co-localization of ADAM23 with Kv1.4. COS7 cells were cotransfected with ADAM23 and Kv1.4-HA (upper), ADAM23 and DPP10-HA (middle), or N-cadherin and Kv1.4-HA (bottom) constructs, respectively. Surface ADAM23, Kv1.4 (HA), DPP10 (HA), and N-cadherin were co-immunostained. The insets show the magnified images of each white square area. Fluorescent intensity profiles along the white lines in the insets are shown (right). Scale bars, 10  $\mu\text{m}$  and 1  $\mu\text{m}$  (insets, magnified).

**(E and F)** Cell surface co-clustering assay. **(E)** Co-expressed Kv1.4-HA (surface) and PSD-95-FLAG showed robust co-cluster formation in contrast to ADAM23 (surface) with Kv1.4-HA or PSD-95-FLAG in COS7 cells. Cotransfection of ADAM23, Kv1.4-HA, and PSD-95-FLAG resulted in large co-cluster formation as observed by cotransfection of Kv1.4-HA and PSD-95-FLAG. **(F)** The co-clustering activity was not seen for surface N-cadherin in the cells cotransfected with Kv1.4-HA and PSD-95-FLAG. The insets show a magnified image of each white square area. Scale bars, 10  $\mu\text{m}$ .

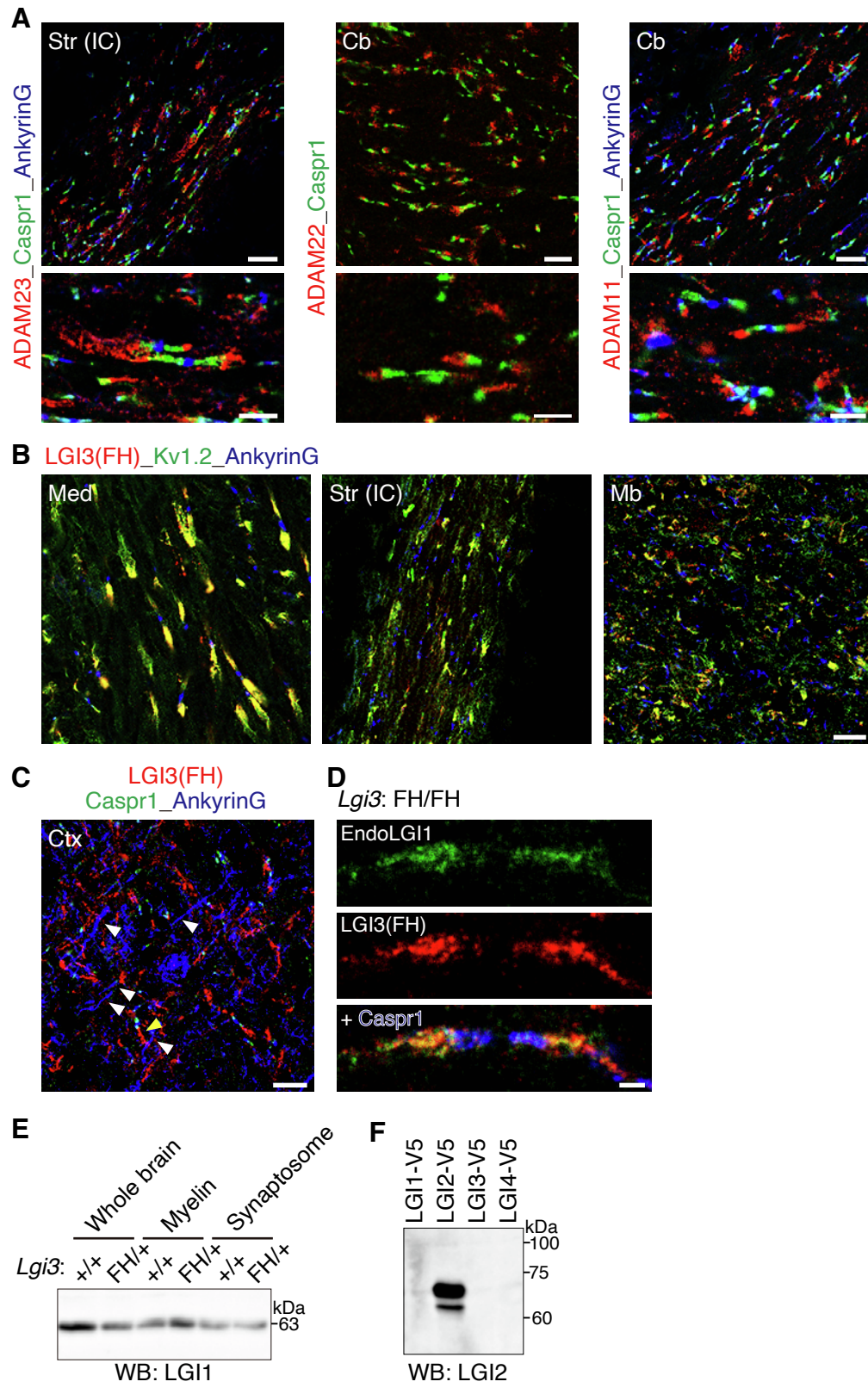


Figure S4 (related to Fig.3)

**Figure S4. Juxtaparanodal localization of LGI3-associated proteins: ADAM23 subfamily, Kv1 channels, and LGI1, Related to Figure 3**

(A) Localization of ADAM23, ADAM22, and ADAM11 at the JXP in the mouse brain. Caspr1 and ankyrinG were co-labeled for a paranodal marker and a nodal marker, respectively. Scale bars, 10  $\mu\text{m}$  (top) and 5  $\mu\text{m}$  (magnified, bottom).

(B) LGI3-FH and Kv1.2 are colocalized at the JXP in the various brain regions of the *Lgi3<sup>FH/FH</sup>* mouse. Scale bar, 10  $\mu\text{m}$ .

(C) LGI3-FH is not identified at the AIS in the cortex of the *Lgi3<sup>FH/FH</sup>* mouse. White arrowheads indicate the AIS determined by the localization of ankyrinG. A yellow arrowhead indicates the representative localization of LGI3 at the JXP. Str, striatum; IC, internal capsule; Cb cerebellum; Med, medulla; Mb, midbrain; Ctx, cortex. Scale bar, 10  $\mu\text{m}$ .

(D) Endogenous LGI1 is colocalized with LGI3-FH at the JXP in the cerebellar white matter of the *Lgi3<sup>FH/FH</sup>* mouse. Scale bar, 1  $\mu\text{m}$ . P100 (A-D) mouse brain slices were used.

(E) LGI1 protein is detected not only in synaptosomal fractions but also in myelin fractions of the mouse brains (P34). The same sample was analyzed in Figure 2D.

(F) The family member-specific reactivity of the LGI2 antibody was confirmed by Western blotting of conditioned medium from HEK293T cells transfected with LGIs-V5.

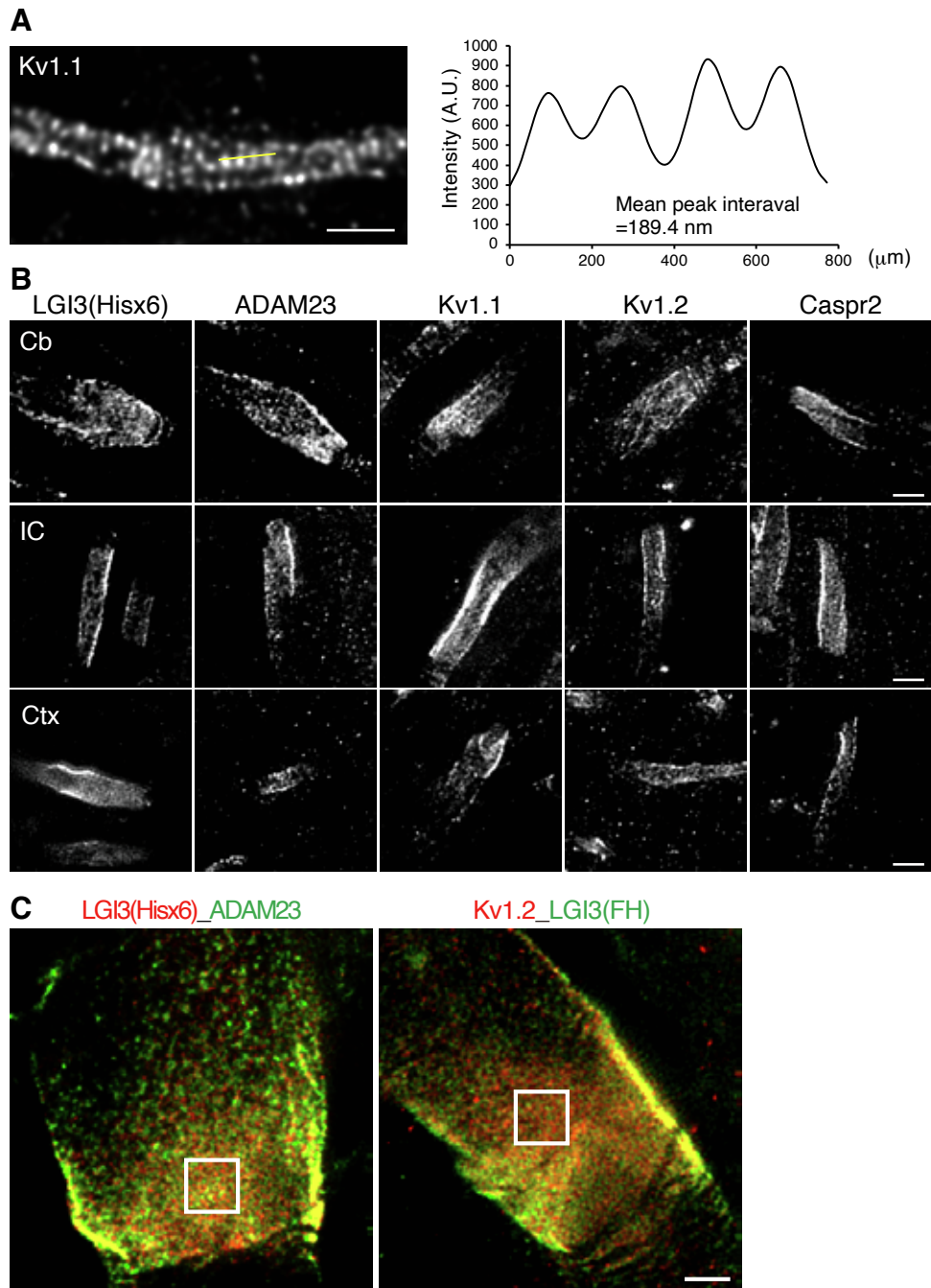


**Figure S5. Superresolution imaging of JXP proteins, Related to Figure 4**

(A) Ladder-like periodic nanoscale localization of Kv1.1 channel at the AIS in rat hippocampal primary cultured neurons. Fluorescent intensity profile along the yellow line and its mean peak interval are shown (right). Scale bars, 1  $\mu\text{m}$ .

(B) STED imaging identifies the nanoscale organizations of LGI3, ADAM23, Kv1.1, Kv1.2, and Caspr2 at the JXP in the various brain regions, which resemble those in medulla (Figure 4B). Cb cerebellum; IC, internal capsule; Ctx, cortex. Scale bars, 1  $\mu\text{m}$ .

(C) Uncropped images of 2C-STED imaging of JXP proteins. The square areas are magnified in Figure 4C. JXP areas of large axons in medulla were observed. Scale bar, 1  $\mu\text{m}$ .

P100 (A-B) *Lgi3*<sup>FH/FH</sup> mouse brain slices were used.

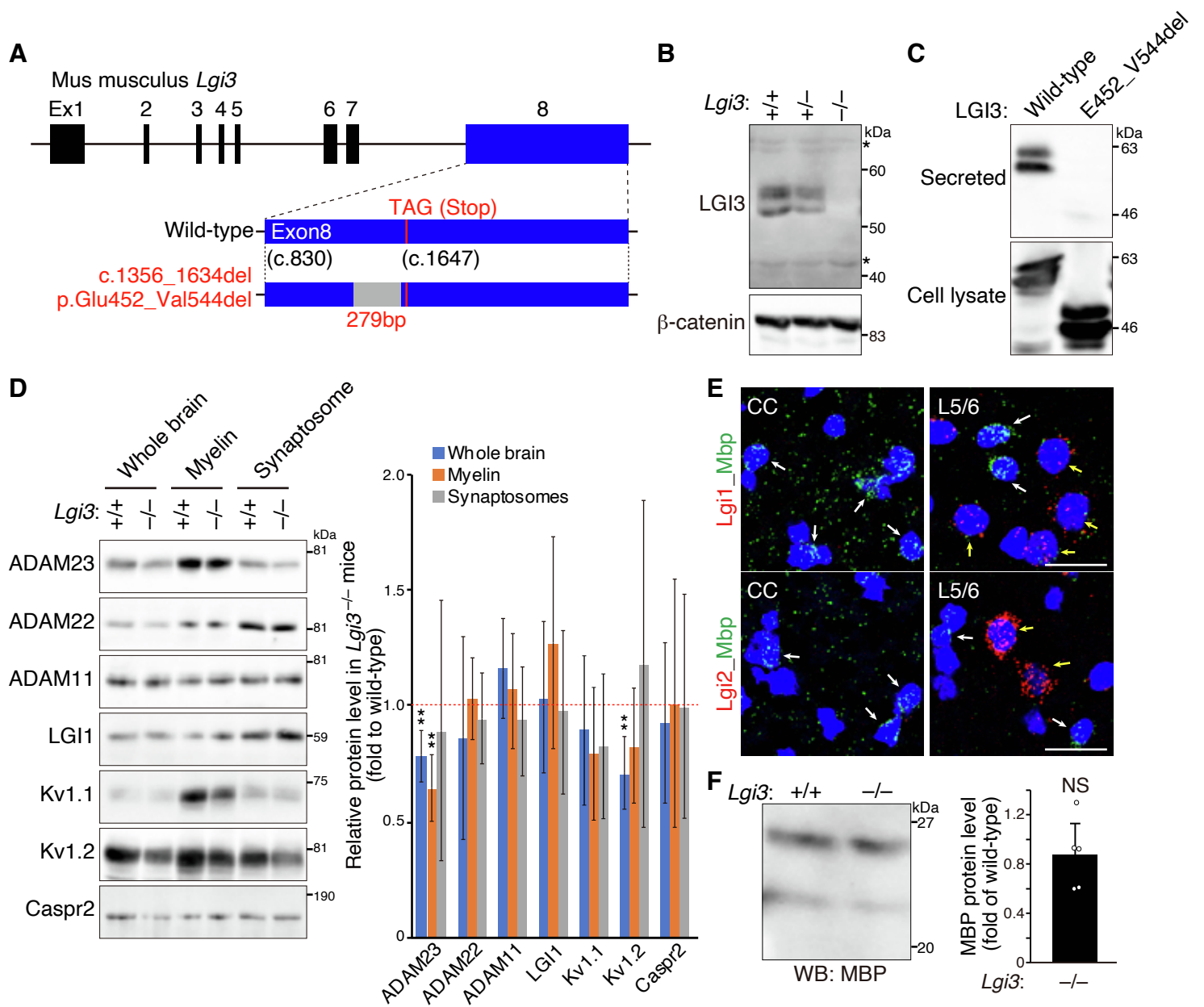


Figure S6 (related to Fig.5)

**Figure S6. Generation and characterization of *Lgi3* loss-of-function mutant mouse (*Lgi3*<sup>-/-</sup> mice), Related to Figure 5**

(A) Schematic presentation of the *Lgi3* deletion mutant allele. A large (279 base pair) in-frame deletion mutation in Exon8 of the *Lgi3* gene causes 93 amino-acid deletion in the EPTP domain of LGI3 protein (Glu452\_Val544del).

(B) LGI3 protein is not detectable in the whole brain lysate of the homozygous *Lgi3* mutant mouse. An asterisk indicates the nonspecifically detected bands on the Western blot. *Lgi3*<sup>+/+</sup>, *Lgi3*<sup>+/-</sup>, and *Lgi3*<sup>-/-</sup> indicate wild-type, heterozygous, and homozygous mutant mice, respectively.

(C) LGI3 E452\_V544 deletion mutant protein is not secreted from HEK293T cells transfected with rat LGI3 constructs.

(D) Loss of LGI3 reduces ADAM23 and Kv1.2 channels in myelin fractions of the young mouse brain (P30). Representative Western blots of the whole mouse brain lysates and subcellular fractions of wild-type (<sup>+/+</sup>) and *Lgi3*<sup>-/-</sup> mice with the indicated antibodies are shown (left). Relative protein levels of each fraction of the *Lgi3*<sup>-/-</sup> mouse brains compared with wild-type control are shown in graph (right). n = 5 mice per genotype. Two-tailed Mann-Whitney U Test. \*\*p < 0.01. mean ± SD.

(E) Loss of LGI3 does not induce *Lgi1* and *Lgi2* mRNA expression in the oligodendrocytes. White arrows, *Mbp*<sup>+</sup>/*Lgi1*<sup>-</sup> or *Mbp*<sup>+</sup>/*Lgi2*<sup>-</sup> cells; yellow arrows, *Mbp*<sup>-</sup>/*Lgi1*<sup>+</sup> or *Mbp*<sup>-</sup>/*Lgi2*<sup>+</sup> cells. Nuclear DNA was stained by DAPI (blue). P100 *Lgi3*<sup>-/-</sup> mouse brain slices were used. Scale bars, 20 μm. CC, corpus callosum; L5/6, cortical layers V and VI.

(F) MBP protein levels are not significantly different between wild-type (<sup>+/+</sup>) and *Lgi3*<sup>-/-</sup> mice (P100). A representative Western blot of MBP protein is shown. Quantification of relative MBP protein levels of the *Lgi3*<sup>-/-</sup> mouse brain compared to wild-type control is shown in graph. n = 5 mice per genotype. Mann-Whitney U test. NS, not significant. mean ± SD.

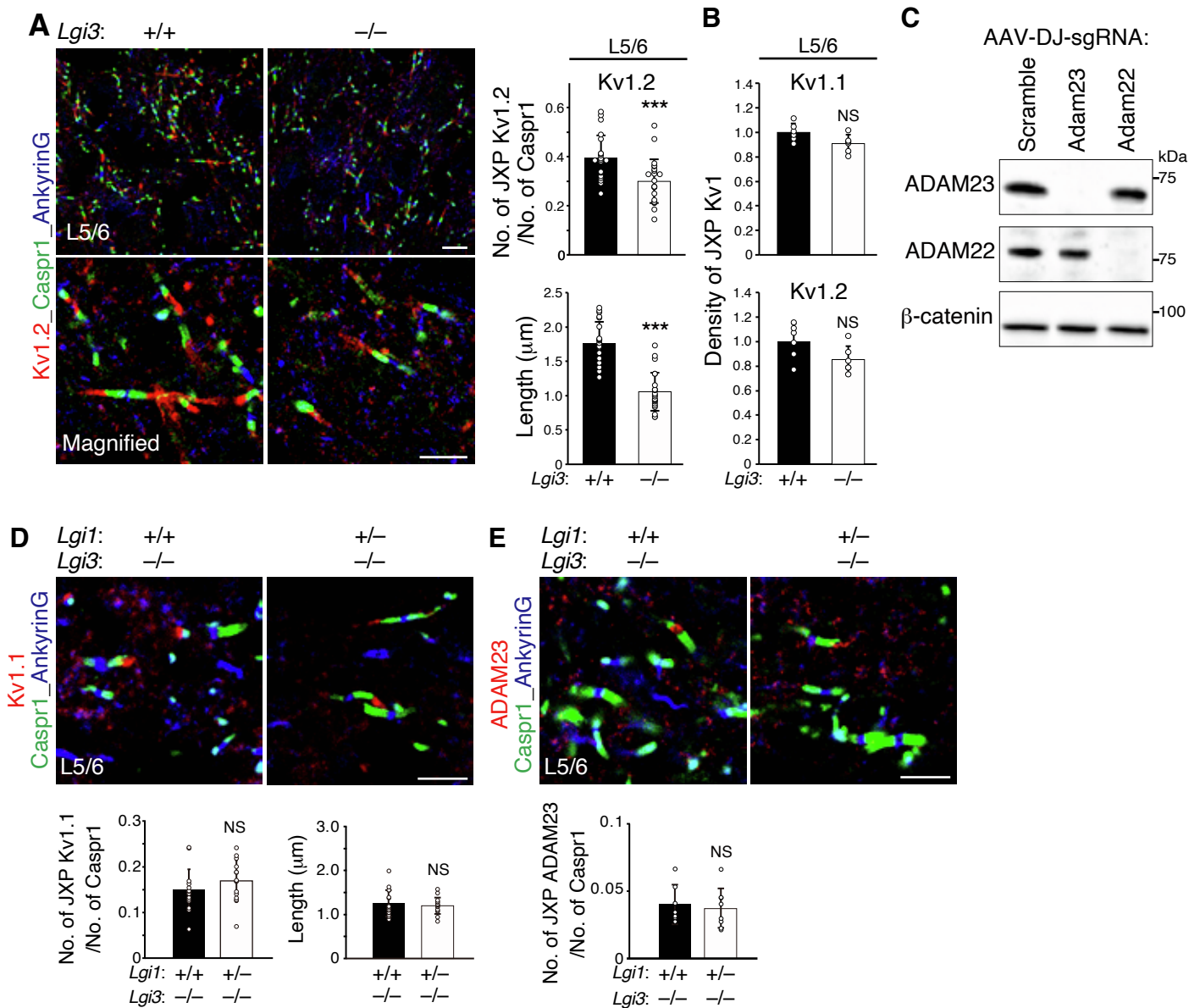


**Figure S7. Loss of LGI3 affects Kv1 channel clustering at the JXP, Related to Figure 6**

(A) Kv1.2 channel clustering at the JXP is impaired by loss of LGI3. Shown are representative images of immunohistochemistry for Kv1.2 channel at the JXP with axonal domain proteins in L5/6 of wild-type (+/+) and *Lgi3*<sup>-/-</sup> mice (left). The number and length of Kv1.2 channel clusters at the JXP are quantitatively compared between genotypes (shown in the graph, right). Scale bars, 10  $\mu\text{m}$  (top) and 5  $\mu\text{m}$  (magnified, bottom). Two-tailed Mann-Whitney U Test. \*\*\* $p < 0.001$ . mean  $\pm$  SD.

(B) The density (mean fluorescence intensity) of JXP Kv1 channels in the cortex is not significantly altered in *Lgi3*<sup>-/-</sup> mice. Two-tailed Mann-Whitney U Test. NS, not significant. mean  $\pm$  SD.

(C) Validation of *Adam23* family gene KO by AAV-mediated CRISPR-Cas9. Primary cultured cortical neurons from *Rosa26*<sup>Cas9/Cas9</sup> knock-in mouse embryos were infected with AAV-DJ carrying sgRNA expressing cassette and a bicistronic mCherry reporter gene at 3 DIV. The targeted *Adam* family genes were specifically reduced in the cultured neuron lysates harvested at 14 DIV. AAV was treated at  $1.0 \times 10^4$  vg /cell.

(D and E) The clustering of Kv1 channels and ADAM23 at the JXP was not significantly different between *Lgi1*<sup>+/+</sup>;*Lgi3*<sup>-/-</sup> and *Lgi1*<sup>+/-</sup>;*Lgi3*<sup>-/-</sup> mice. Shown are representative images of immunohistochemistry for Kv1.1 channel (D) and ADAM23 (E) clusters at the JXP in the cortex (L5/6). The number and length of juxtapanodal Kv1.1 channel and ADAM23 clusters are quantitatively compared between genotypes (shown in the graph, right).  $n = 2$  mice per genotype. Mann-Whitney U Test. NS, not significant. mean  $\pm$  SD. Scale bars, 5  $\mu\text{m}$ .

**Figure S7 (related to Fig.6)**

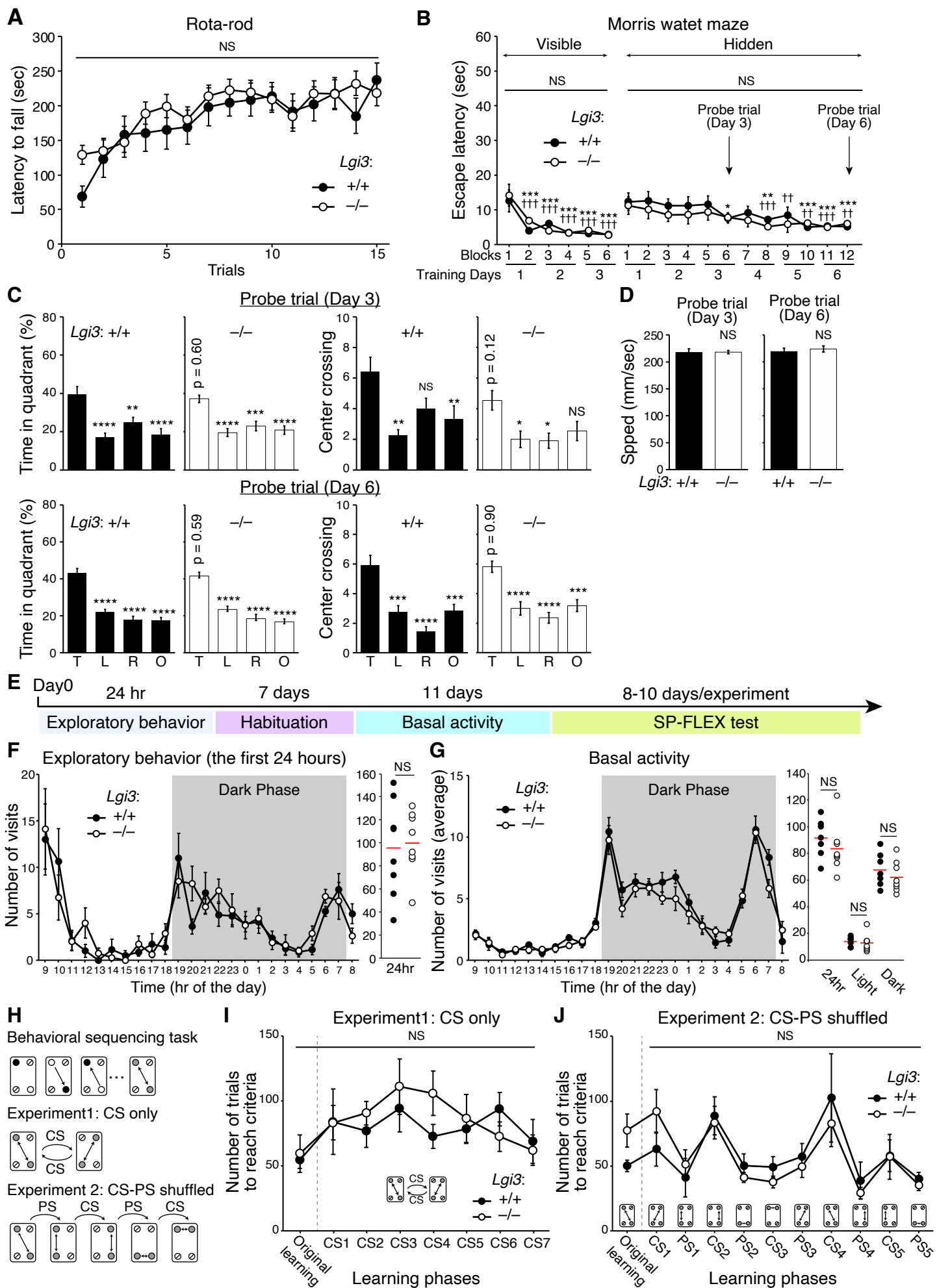


Figure S8

## Figure S8. Behavioral analysis of *Lgi3*<sup>-/-</sup> mice

(A) Motor coordination and learning are intact in the *Lgi3*<sup>-/-</sup> mice (Rota-rod test). Mice were placed on an accelerating rotating rod. The speed of the rod is accelerated from 5 rpm to 40 rpm over 300 sec. Latency to fall of 15 trials of three consecutive days is shown in the graph. n = 13 per genotype. Two-way repeated measures ANOVA. Genotype effect,  $F_{(1, 24)} = 0.37$ ,  $p = 0.55$ . NS, not significant. mean  $\pm$  SEM.

(B, C, and D) Spatial recognition and memory of *Lgi3*<sup>-/-</sup> mice were examined by the Morris water maze tasks. (B) Escape latencies in the visible platform trials (six blocks of the first three days) and the following hidden platform trials (twelve blocks of the six days) of *Lgi3*<sup>-/-</sup> mice were compared to the wild-type. Two-way repeated measures ANOVA. Visible platform trial: interaction,  $F_{(5, 105)} = 0.90$ ,  $p = 0.49$ ; genotype,  $F_{(1, 21)} = 0.31$ ,  $p = 0.58$ ; blocks of trial effect,  $F_{(11, 105)} = 19.22$ ,  $p < 0.001$ ; Hidden platform trial: interaction,  $F_{(11, 231)} = 0.65$ ,  $p = 0.78$ ; genotype,  $F_{(1, 21)} = 0.82$ ,  $p = 0.37$ ; blocks of trial effect,  $F_{(11, 231)} = 7.14$ ,  $p < 0.001$ . NS, not significant. Bonferroni's post hoc test. \* $p < 0.05$ , \*\* $p < 0.01$ , \*\*\* $p < 0.001$  (wild-type); † $p < 0.05$ , †† $p < 0.01$ , ††† $p < 0.001$  (*Lgi3*<sup>-/-</sup>) (vs the first trial in each training). mean  $\pm$  SEM. (C) Probe trials were performed on days 3 and 6 after training trials. Percentage time in each quadrant (left) and the number of center crossings of the hypothetical platform (right) were analyzed. One-way ANOVA post hoc Tukey's test (vs target in each genotype). NS, not significant, \* $p < 0.05$ , \*\* $p < 0.01$ , \*\*\* $p < 0.001$ , and \*\*\*\* $p < 0.0001$ . P-values in the graph show the differences in the target quadrant or center crossing between wild-type and *Lgi3*<sup>-/-</sup> mice (Student t-test). mean  $\pm$  SEM. T, target quadrant; L, left quadrant; R, right quadrant; O, opposite quadrant. (D) Swimming speed measured for 60 sec in the probe trials on days 3 and 6 was not significantly different between genotypes (Student t-test). mean  $\pm$  SEM. (B-D) n = 11 (wild-type mice) and n = 12 (*Lgi3*<sup>-/-</sup> mice).

(E) Experimental schedule of behavioral analysis using IntelliCage. SP-FLEX test, Self-paced behavioral sequencing learning and behavioral FLEXibility test.

(F and G) Exploratory behavior (F) and basal activity (G) of *Lgi3*<sup>-/-</sup> mice and wild-type control mice were assessed. The total number of corner visits during the 24 hr of the exploratory behavior task (F, right) and the mean number of corner visits for the 24-hour, light, and dark period are shown in graph (G, right), respectively. Student t-test. NS, not significant. Red lines represent the mean value. (F) n = 8 mice per genotype. (G) n = 7 (wild-type mice) and n = 8 (*Lgi3*<sup>-/-</sup> mice). mean  $\pm$  SEM.

(H) Behavioral sequencing task scheme for self-paced learning and flexibility, showing opposite rewarded corners where the mouse has to go back and forth. In the complete shift (CS)-only task, the diagonally opposite rewarded corners are alternated sequentially with the other, upon achieving the successful visit-rate criterion at one diagonal. In the shuffled task, CS is alternated with the partial shift (PS) task, where only one of the two previously rewarded corners is switched with a nonrewarded corner. Black-filled circle, rewarded corner (active); Open circle, rewarded corner (inactive); crossed-out circle, non-rewarded corner; gray-filled circles connected with double arrow, rewarding sequence.

(I and J) No significant differences were observed between genotypes in the CS-only and CS-PS-shuffled SP-FLEX experiments. Two-way repeated-measures ANOVA. CS-only (I): genotype effect,  $F_{(1, 13)} = 0.26$ ,  $p = 0.62$ , NS, not significant. n = 7 (wild-type mice) and n = 8 (*Lgi3*<sup>-/-</sup> mice); CS-PS-shuffled (J), genotype effect,  $F_{(1, 12)} = 0.067$ ,  $p = 0.80$ . n = 6 (wild-type mice) and n = 8 (*Lgi3*<sup>-/-</sup> mice). mean  $\pm$  SEM.

**Table S1. Summary of FISH analysis of *Lgi1*, *Lgi2*, and *Lgi3* expression in oligodendrocytes in the mouse brain, Related to Figure 1**

	<i>Lgi3</i> <sup>+</sup> /DAPI <sup>+</sup> cells (%)	<i>Mbp</i> <sup>+</sup> /DAPI <sup>+</sup> cells (%)	<i>Mbp</i> <sup>+</sup> / <i>Lgi3</i> <sup>+</sup> cells (%)	<i>Lgi3</i> <sup>+</sup> / <i>Mbp</i> <sup>+</sup> cells (%)	<i>Lgi1</i> <sup>+</sup> /DAPI <sup>+</sup> cells (%)	<i>Mbp</i> <sup>+</sup> / <i>Lgi1</i> <sup>+</sup> cells (%)	<i>Lgi2</i> <sup>+</sup> /DAPI <sup>+</sup> cells (%)	<i>Mbp</i> <sup>+</sup> / <i>Lgi2</i> <sup>+</sup> cells (%)
Corpus Callosum	69.8	65.3	83.8	89.7	N.D.	N.D.	N.D.	N.D.
Internal capsule (Striatum)	52.8	55.7	92.9	88.1	N.D.	N.D.	N.D.	N.D.
Cerebellum (White matter)	46.9	45.3	86.3	89.1	2.0	N.D.	N.D.	N.D.
Cortex layer 5/6	42.3	22.7	51.0	87.9	45.8	N.D.	23.2	N.D.
Cortex layer 2/3	49.2	5.4	10.6	100.0	51.4	N.D.	21.6	N.D.
Thalamus	54.8	24.5	43.0	94.6	25.2	N.D.	N.A.* <sup>2</sup>	N.D.
Medulla	58.8* <sup>1</sup>	29.5	45.2* <sup>1</sup>	89.0	28.5	N.D.	N.A.* <sup>2</sup>	N.D.

The average percentage of two independent experiments is shown (P125, C57BL/6 mouse brains).

\*1: The subregions in the medulla, in which *Lgi3*<sup>+</sup> cells are locally clustered, are excluded from the calculation.

\*2: *Lgi2*<sup>+</sup> cells are not distributed uniformly in the thalamus and medulla.

N.D., not detected; N.A., not applicable.

**Table S3. Kv1 channel peptides identified in LGI3-mediated protein complexes by proteomic analysis, Related to Figure 3**

	Amino acid sequence*	# PSMs
Kcna1 (Kv1.1)	[R].NRPSFDAILYQSGGR.[LI]	8
	[R].NEYFFDR.[NH]	4
	[R].RPVNVPLDMFSEEIK.[F]	4
	[R].QVWLLFEYPESGPAR.[VGI]	4
	[M].TVMSGENADEASTAPGHPQDGSYPR.[Q]	1
	[R].VVINISGLR.[F]	4
	[K].TLAQFPNTLLGNPK.[K]	1
	[K].GLQILGQTLK.[A]	2
	[K].FYELGEEAMEK.[F]	1
[KR].FREDEGFIK.[E]	1	
Kcna2 (Kv1.2)	[R].NRPSFDAILYQSGGR.[LI]	8
	[R].NEYFFDR.[NH]	4
	[R].RPVNVPIDIFSEEIR.[F]	16
	[R].QVWLLFEYPESGPAR.[VGI]	4
	[M].TVATGDPVDEAAAALPGHPQDQTYDPEADHECCER.[V]	4
	[R].VVINISGLR.[F]	4
	[K].TLAQFPETLLGDPK.[K]	4
	[K].EEERPLPENEFQR.[Q]	3
	[R].ETEGEEQAQYLQVTSCP.[I]	2
	[K].GLQILGQTLK.[A]	2
[R].FYELGEEAMEMFR.[E]	2	
Kcna3 (Kv1.3)	[R].NRPSFDAILYQSGGR.[LI]	8
	[R].NEYFFDR.[NH]	4
	[R].RPVNVPIDIFSEEIR.[F]	16
	[R].QVWLLFEYPESGPAR.[VGI]	4
	[R].VVINISGLR.[F]	4
	[K].GLQILGQTLK.[A]	2

Kcna4	[R].NRPSFDAILYYSQSGGR.[LI]	8
(Kv1.4)	[R].NEYFFDR.[NH]	4
Kcna6	[R].NRPSFDAILYYSQSGGR.[LI]	8
(Kv1.6)	[R].NEYFFDR.[NH]	4
	[R].QVWLLFEYPESSGPARG.[VGI]	4
Kcna10	[R].NEYFFDR.[NH]	4
(Kv1.8)	[K].GLQILGQTLK.[A]	2

\* The peptide sequences shown in black indicate uniquely identified peptides, while the peptide sequences shared between different Kv1 channels are shown by the same color other than black.

PSM, peptide-spectrum match.

**Table S4. Electrophysiological properties of L5a PCs,  
Related to Figure 7**

	Wild-type (control)	<i>Lgi3</i> <sup>-/-</sup>
Resting membrane potentials (mV)	-70.7 ± 4.2	-71.9 ± 5.2
Input resistance (MΩ)	96.2 ± 25.7	92.7 ± 31.0
Spike threshold (mV)	-42.7 ± 3.1	-42.5 ± 5.6
Spike height (mV)	81.5 ± 7.5	79.1 ± 8.7
Spike width (msec)	3.6 ± 1.1	3.9 ± 1.4

**Table S5. Electrophysiological properties of L2/3 PCs,  
Related to Figure 7**

	Wild-type (control)	<i>Lgi3</i> <sup>-/-</sup>
Resting membrane potentials (mV)	-79.2 ± 1.8	-78.8 ± 1.5
Input resistance (MΩ)	72.1 ± 19.7	71.6 ± 21.0
Spike threshold (mV)	-39.9 ± 1.9	-40.0 ± 2.1
Spike height (mV)	83.7 ± 4.1	83.4 ± 7.3
Spike width (msec)	3.7 ± 0.4	3.8 ± 0.5